Progress In Electromagnetics Research, Vol. 125, 237–254, 2012

DETECTION OF CORONA AND DRY-BAND ARC DISCHARGES ON NANO-COMPOSITE EPOXY INSULATORS USING RF SENSING

S. C. Fernando*, K. L. Wong, and W. S. T. Rowe

School of Electrical and Computer Engineering, RMIT University, Melbourne, VIC 3001, Australia

Abstract—RF radiation due to corona and dry-band arc discharges have been observed using an antenna. Variations in radiated energy were observed due to change in the distance between two water droplets, the contact angle and the volume of the droplets, and the condition of the insulator surface. Changes in the frequency spectrum within the 800 MHz–900 MHz and 1.25 GHz–1.4 GHz frequency bands have been used to identify the transition from corona discharge to dry-band arc discharge. The 800 MHz–900 MHz emission band has also been used to monitor the condition of the insulator. These findings highlight the potential for RF sensing in the identification of partial discharges and insulator condition monitoring.

1. INTRODUCTION

Partial discharge (PD) is a key precursor to catastrophic failure events in high voltage distribution networks. Consequences of PD can include pole top fires and bush fires, which can cause damage to power infrastructure and the surrounding environment worth of millions of dollars. PD can occur in the form of cavity discharges and surface discharges. Insulator manufacturing has evolved to mitigate partial discharge in insulators. Ceramic materials have been used in the past for high voltage (HV) insulator manufacturing. However manufactures now commonly use nano-composite materials due to their hydrophobic properties and high durability [1]. Quality control methods used in the insulator manufacturing process have rendered cavity discharges from nano-composite insulators almost non-existent. However some forms of surface discharges such as corona and dry-band arc discharges are

Received 12 January 2012, Accepted 12 February 2012, Scheduled 28 February 2012

* Corresponding author: Sahan Chathura Fernando (sahan.fernando@rmit.edu.au).

still common, particularly when the surface of the insulator is wet. Insulators can degrade due to insulator pollution, ultraviolet radiation, acid rain and surface discharges. Of these causes, surface discharges have a high impact on insulator degradation [2]. Corona discharge initiates when a water droplet on the surface of an insulator starts to change the shape only under electrical stress [3]. Under heavy corona discharge, the insulator will degrade and the insulation material will lose its hydrophobicity [4]. This loss of hydrophobicity leads to imminent dry-band arcing. Extensive levels of dry-band arcing are also detrimental to insulator condition due to the significant amount of current transmission, potentially leading to catastrophic failure [5, 6].

The use of leakage current characterization for estimating the condition of the insulators, and hence detecting the dry-band arc discharges has previously been reported [7, 8]. Measuring the magnitude of the PD has also been discussed as a possible method of detecting the transition from corona discharge to dry-band arcing on the insulator [9]. This detection method must be performed inside a laboratory, meaning the insulator needs to be removed from the electrical power grid. Due to the lack of an online, non-contact detection method to identify failing insulators caused by dry-band arcing, power companies cannot identify a damaged insulator until the insulator has completely failed. It has been proposed that RF sensors can be used for online PD detection [10].

A UHF technique to identify the discharge initiated by a liquid droplet on epoxy nano-composite insulation material was proposed in previous studies [11]. Discharges using a single NH_4Cl droplet under AC voltage were investigated with different percentages of nano-composites. The corona discharge between two water droplets has been studied previously [12–14]. However, the experiments in [11–14] did not address the radiated UHF signal caused by corona discharge between two water droplets, dry-band arcing, and the differences between the two.

This paper measures and evaluates the radiated frequency spectrums ranging from 0 GHz–2.5 GHz due to corona discharge between two water droplets, as well as the resulting dry-band arcing. Parameters such as the droplet size and separation are varied to examine their influence on the resulting radiation. The potential for the detection of transition between corona and dry-band arcing based on the differences in the frequency spectrums generated by both discharges is also determined. The condition of the HV insulator is assessed using the RF emissions from successive sets of discharges on the same insulator location. These results highlight the potential of this RF sensing technique for insulator condition monitoring.

2. EXPERIMENTAL METHOD

Two water droplets of Melbourne (Australia) tap water which have the same volume were placed on a nano-composite epoxy sample, as seen in Figure 1. Both water droplets were connected to metal electrodes, one of them was grounded whilst the other was connected to a 5 kV 50 Hz AC voltage supply (shown in the experimental setup of Figure 2). Signals emitted from corona and dry-band arcing were observed using wideband horn antenna located 1 m away from the discharge source. The 1 m distance was chosen to ensure adequate signal strength was received by the antenna [15]. A Tektronix real-time oscilloscope with a 5 GS/s sampling rate and 1 GHz bandwidth was used to analyze the measured signal. Due to the stochastic nature of high voltage discharges, twenty data samples were collected for each of seven different locations on an epoxy sample for each test. The recorded data was then converted via a Fast Fourier Transformation (FFT) to the frequency domain over the range of 0 GHz–2.5 GHz.

In practical scenarios, water droplets formed on the high voltage insulator are likely to be of different volume and have varying distances between each other. Therefore, a set of results was collected for 0.4 mL water droplets having a distance between electrodes of 1.5 cm, 2 cm and 2.5 cm. A second set of data was observed by varying the size of the water droplets from 0.2 mL to 0.8 mL in 0.2 mL steps, providing a wide coverage of droplet contact angles with the insulator surface, whilst keeping the distance between electrodes at 2 cm. To monitor changes to the frequency spectrum due to the degradation of the insulator, radiated signals were observed for repeated discharges at the same physical location on the insulator sample surface.

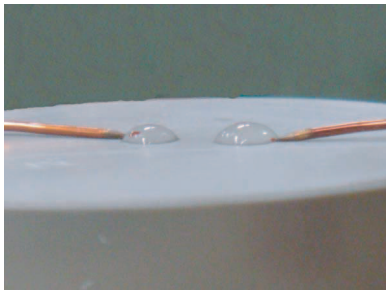

Figure 1. Two 0.4 mL water droplets on the epoxy nano-composite sample before corona discharge.

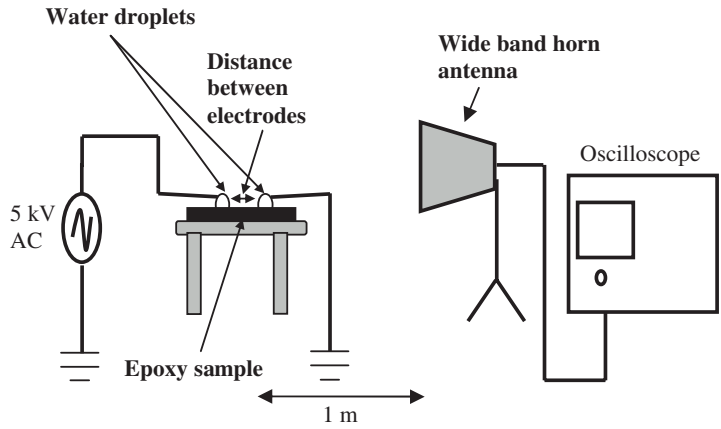

Figure 2. Experimental setup of the high voltage discharge between two water droplets.

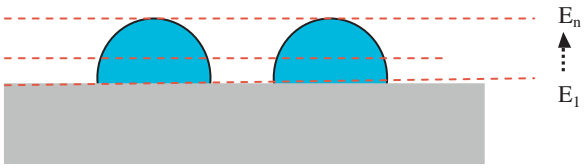

Figure 3. Electric field distribution lines to explain the initiation of corona discharge.

3. RESULTS AND DISCUSSION

3.1. Initialisation of Corona Discharge between Two Water Droplets

Water droplets formed on the surface of electrical insulators result in a disturbed electric field distribution around the insulator [16, 17]. The electric field variation surrounding the water droplets when under a constant electric field E_o is discussed in [17–20]. Electric field distributions along the lines of equal distance from the insulator surface (E_1 to E_n in Figure 3) are defined. The variation in electric fields is described as an electric field enhancement factor (E_{efn}), relative to each line (Equations (1) and (2)). Corona discharge will initiate where E_{efn} is maximum [18]. However the value of n for maximum E_{efn} will change with the contact angle of the water droplet [20]. Hence path of the discharge will also vary with the contact angle, as shown in Figure 4.

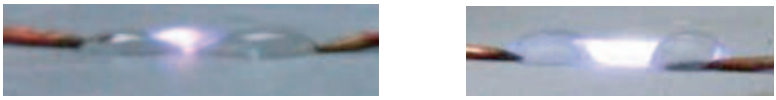

(a) (b)

Figure 4. Discharge between (a) 0.4 mL water droplets on epoxy surface (approximate contact angle of 71 degrees) (b) 0.4 mL water droplet on silicon-rubber surface (approximate contact angle of 90 degrees) [10].

$$E_{\text{efn}} = E_n / E_o \tag{1}$$

E_{efn} = Electric Field Enhancement Factor at nth line
E_n = Electric Field along the nth line
where

$$E_o = V/d \tag{2}$$

V = Applied voltage
d = Distance between electrodes.

3.2. RF Signature for Corona and Dry-band Arcing Discharges for Different Distances between Two Water Droplets

In real life scenarios a HV insulator is under constant AC voltage and the distance between two adjacent water droplets is random. An investigation into the effect of the distance between water droplets on the RF signature from corona and dry-band arcing was performed. The distance between water droplets is linked to the magnitude of the electric field when the applied voltage is constant. The electric field magnitude applied was 3.3 kV/cm, 2.5 kV/cm and 2 kV/cm for corresponding distances between electrodes of 1.5 cm, 2 cm and 2.5 cm respectively.

As seen in Figure 5, there is a notable difference between the RF spectrums for corona discharge and dry-band arcing for each of the three electrode separations. This variation can be clearly observed in the 750 MHz–1500 MHz region in all three cases. Of particular note is the region around 800 MHz–900 MHz, where dry-band arc discharge shows higher magnitude of RF radiation as compared to corona discharge. The opposite activity can be observed for the 1.25 GHz–1.4 GHz band, where corona discharge emits with a higher magnitude. These effects are examined in more detail in Figure 6, where the average voltage spectral density is portrayed in these bands.

The electric field between the electrodes has reduced when increasing the distance between them. Therefore the electric field

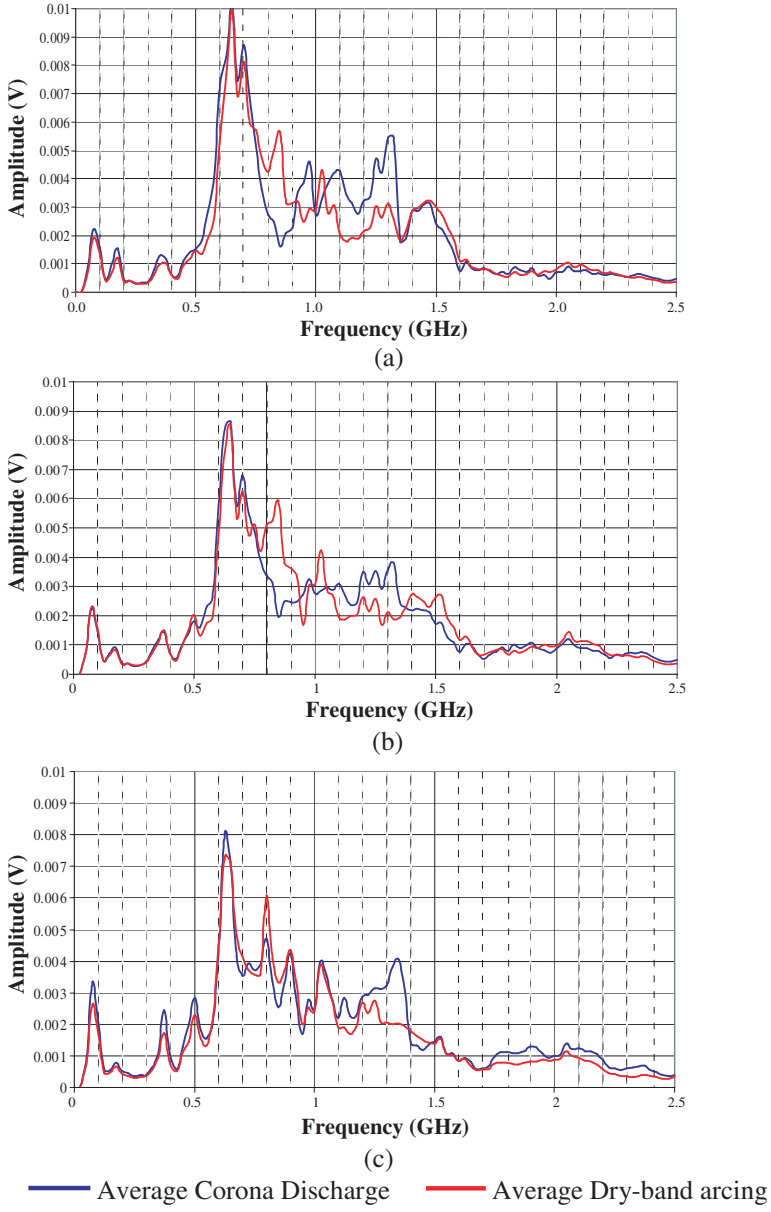

Figure 5. Average corona and dry-band arcing spectrum between two 0.4 mL water droplets for different distances between electrodes. (a) 1.5 cm. (b) 2 cm. (c) 2.5 cm.

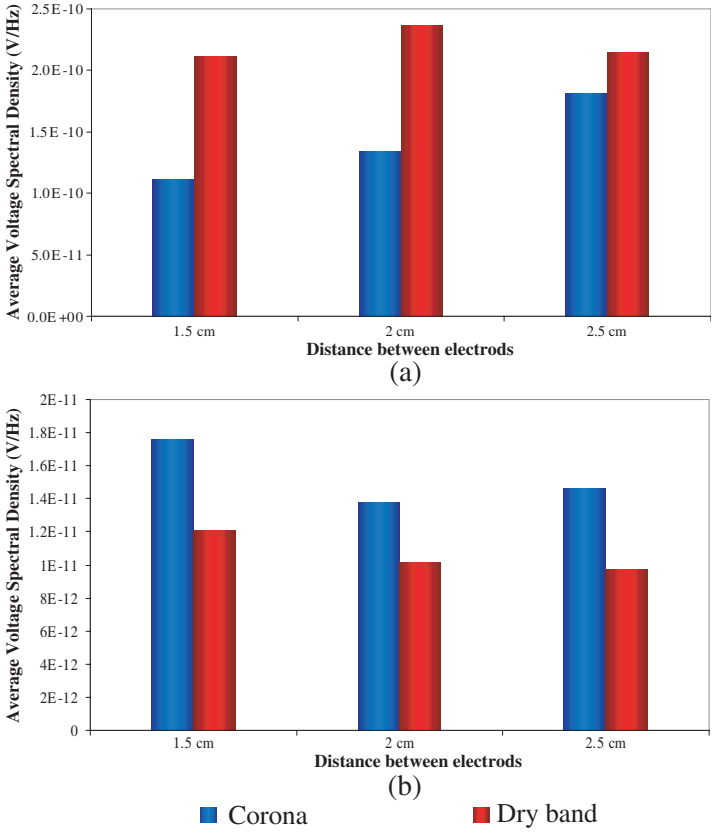

Figure 6. Average Voltage Spectral Density for Corona and Dry-band arc discharges for different distances between electrodes for (a) frequency band of 800 MHz–900 MHz (b) frequency band of 1.25 GHz–1.4 GHz.

between the two water droplets has also reduced, causing a decrease in the overall magnitude of the corona discharge between the two water droplets. Consequently, the level of radiated energy due to corona and dry-band arcing has reduced for the whole frequency band from 0 GHz–2.5 GHz, as shown in Figure 7.

3.3. RF Signature for Corona and Dry-band Arcing Discharges for Water Droplets of Different Volume

Previous research has shown that the water droplets under constant electrical stress will enhance the nearby electric field [18]. To

understand the extent of this effect on the RF signature of corona discharge and dry band arcing, droplets with different volumes were investigated whilst the distance between electrodes was kept constant at 2 cm. Each water droplet was photographed (Figure 8) to observe changes to the contact angle with the volume of water.

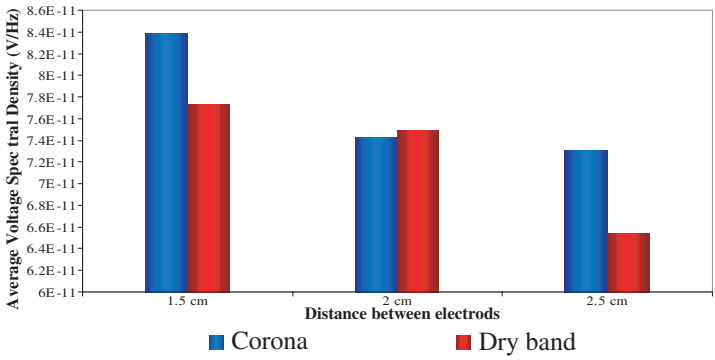

Figure 7. Average Voltage Spectral Density for Corona and Dry-band arc discharges for different distances between electrodes for frequency spectrum of 0 GHz–2.5 GHz.

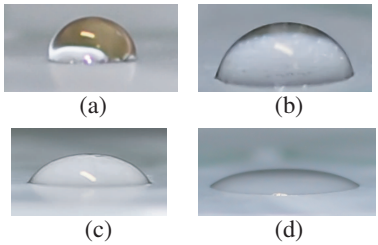

Figure 8. Water droplets of different volumes on epoxy nano-composite insulators. (a) 0.2 mL. (b) 0.4 mL. (c) 0.6 mL. (d) 0.8 mL.

Table 1. Approximate contact angle of the water droplets and the time until breakdown.

Volume of the droplets	Contact Angle (Degrees)	Time until breakdown (minutes)
0.2 mL	89	14.50
0.4 mL	71	9.36
0.6 mL	52	6.26
0.8 mL	23	4.17

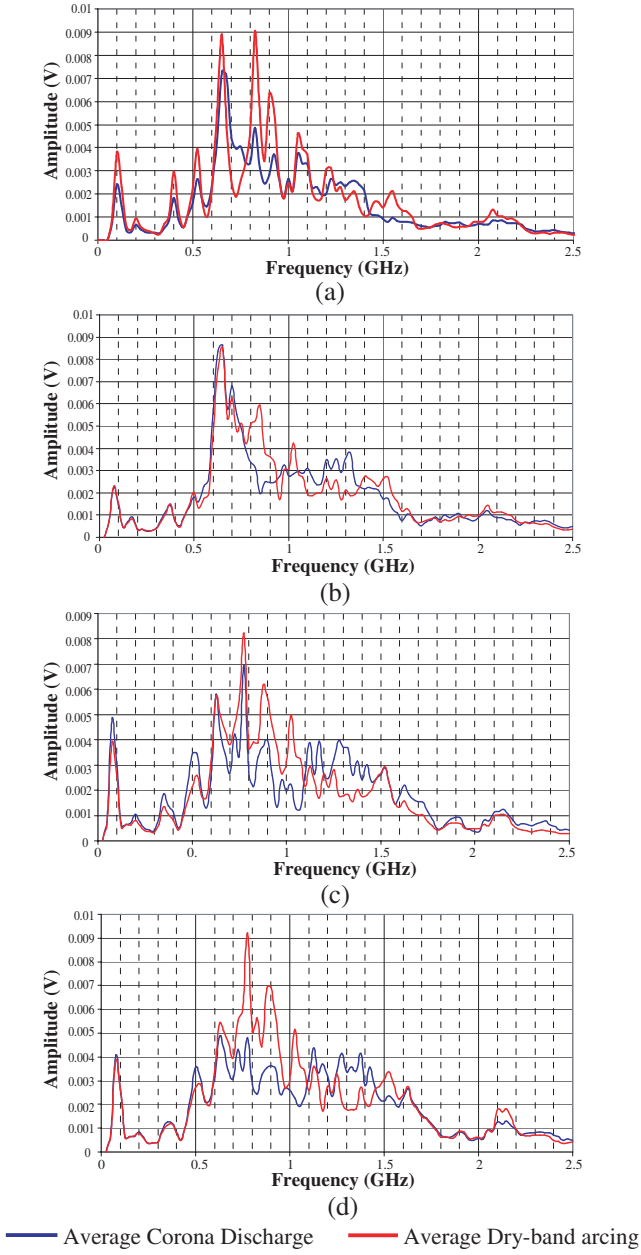

Figure 9. Average corona and dry-band arcing between two water droplets of different volumes for a constant distance (2 cm) between electrodes: (a) 0.2 mL. (b) 0.4 mL. (c) 0.6 mL. (d) 0.8 mL.

The contact angle of the water droplet (and hence the shape of the droplet) changes with increasing volume of the droplet [19]. It also changes with the hydrophobicity level of the material. A change in droplet volume also alters the radius of water droplet footprint. Hence the distance which separates two water droplets in the experimental setup of Figure 1 changes from approximately 1.2 cm to 0.5 cm for volumes of 0.2 mL to 0.8 mL respectively. This also results in a reduction in the time taken for breakdown to initiate. Table 1 shows the approximate contact angle measured using the photographs of the water droplets shown in Figure 8 and image processing software, and the time taken until breakdown occurs.

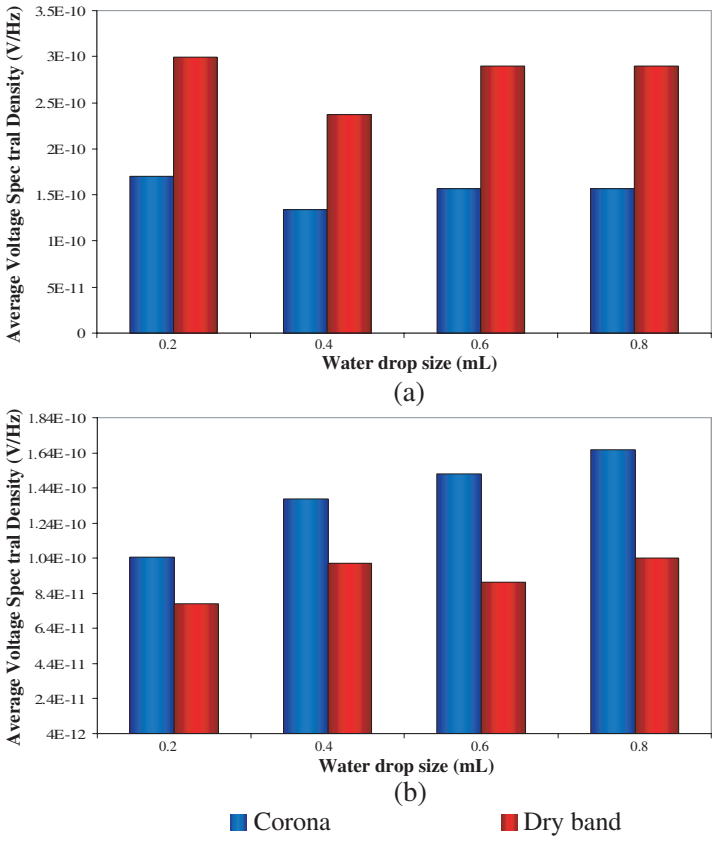

Figure 10. Average Voltage Spectral Density for Corona and Dry-band arc discharges for different water droplet volumes. (a) Frequency band of 800 MHz–900 MHz. (b) Frequency band of 1.25 GHz–1.4 GHz.

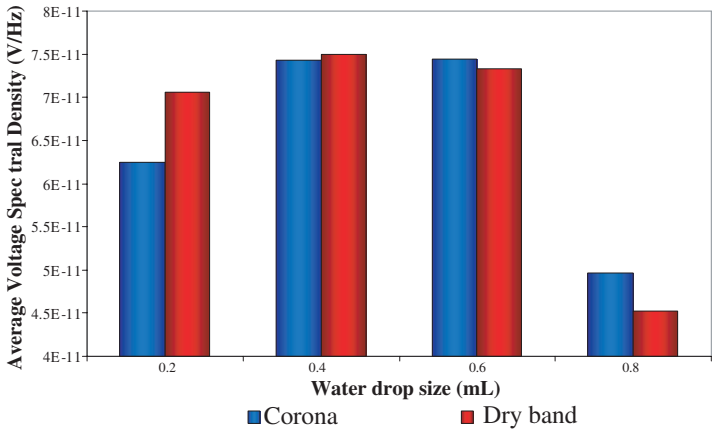

Figure 11. Average Voltage Spectral Density for Corona and Dry-band arc discharges for different contents of water droplets for frequency spectrum of 0 GHz–2.5 GHz.

Figure 9 displays the frequency spectrums for corona and dry-band arc discharges when changing the volume of both water droplets between 0.2 mL, 0.4 mL, 0.6 mL and 0.8 mL. Again a notable difference between the RF spectrum for corona discharge and dry-band arcing has been observed in the frequency band of 750 MHz–1500 MHz for all four cases. Concentrating on the 800 MHz–900 MHz band, dry-band arc discharge again shows a higher magnitude of RF radiation energy than corona discharge, while corona discharge exceeds dry-band arc discharge in the 1.25 GHz–1.4 GHz band. This activity (depicted in Figure 10) is similar to that observed and discussed in Subsection 3.2. Sensing the radiated energy in these bands could potentially provide a non-contact method of discriminating between corona discharges and dry-band arcing.

Guan et al. [18] has shown using electromagnetic simulation model that increasing the contact angle of the water droplet by changing its volume, the electric field enhancement due to corona discharge first increases, and then decreases, reaching a peak value between 40 to 60 degrees. The total energy radiated from both corona and dry-band arc discharges shown in Figure 11 displays a rapid increase when the droplet volume decreased from 0.8 mL to 0.6 mL, corresponding to an increase in contact angle from 23 to 52 degrees. As the droplet volume changed from 0.6 mL to 0.4 mL the radiated energy held relatively constant, and a further decrease in volume to 0.2 mL showed a noticeable drop in radiation, particularly for corona discharge. Hence the experimental results for corona discharge showed in Figure 11 bear

reasonable resemblance to the findings of [18].

The local electric field distribution has been shown to vary with the changes to the shape of a water droplet [20]. The changes in the electric field distribution with change in contact angle of the two water droplets may have an effect on the water droplet deformation, hence affecting the creation of dry bands [21]. This in turn will have influence the number of dry bands created. Consequently the overall magnitude of the radiated energy pattern from dry-band arc discharge follows a similar trend as from corona discharge (Figure 11) when increasing the water content of the droplets, resulting from the change in contact angle.

3.4. RF Signature due to Repetition of Corona and Dry-band Arc Discharges at the Same Surface Location on the Epoxy Sample

Repetitive corona and dry-band arc discharges cause damage to an insulator surface and reduces its hydrophobicity [22]. This has an impact on the contact angle and footprint of the water droplet. An experimental investigation was conducted to analyze the relationship between RF radiation due to discharge activity, and the associated degradation of the surface of the insulator. Seven sets of corona and dry band arc discharge experiments were conducted at the same location on a nano-composite epoxy sample using two 0.4 mL water droplets 2 cm apart.

The radiated RF spectrums from the first four experimental stages are shown in Figure 12. For these stages, both corona and dry-band arc discharges have been observed. Only dry-band arc discharges were observed from the 5th to 7th stages. The spectral results are not shown for these stages, as they remain similar to the dry-band arc discharge at the 4th stage. The absence of the corona discharge in these latter stages is due to the loss of hydrophobicity of the insulator surface. This creates water bridging between two droplets even before the AC voltage can be applied. As was seen previously, the most significant variation between RF signatures for corona and dry-band arc discharge in Figure 12 can be observed between approximately 750 MHz–1500 MHz.

The detected radiation for corona and dry-band arc discharges in 800 MHz–900 MHz and 1.25 GHz–1.4 GHz bands are shown in Figure 13. In the 800 MHz–900 MHz frequency band of Figure 13(a), Stages 1 and 2 show higher average voltage spectral densities from dry-band arc discharge, while Stages 3 and 4 show a higher level from corona discharge. In the 1.25 GHz–1.4 GHz frequency band of Figure 13(b), Stages 1, 2 and 4 show higher level of radiated energy

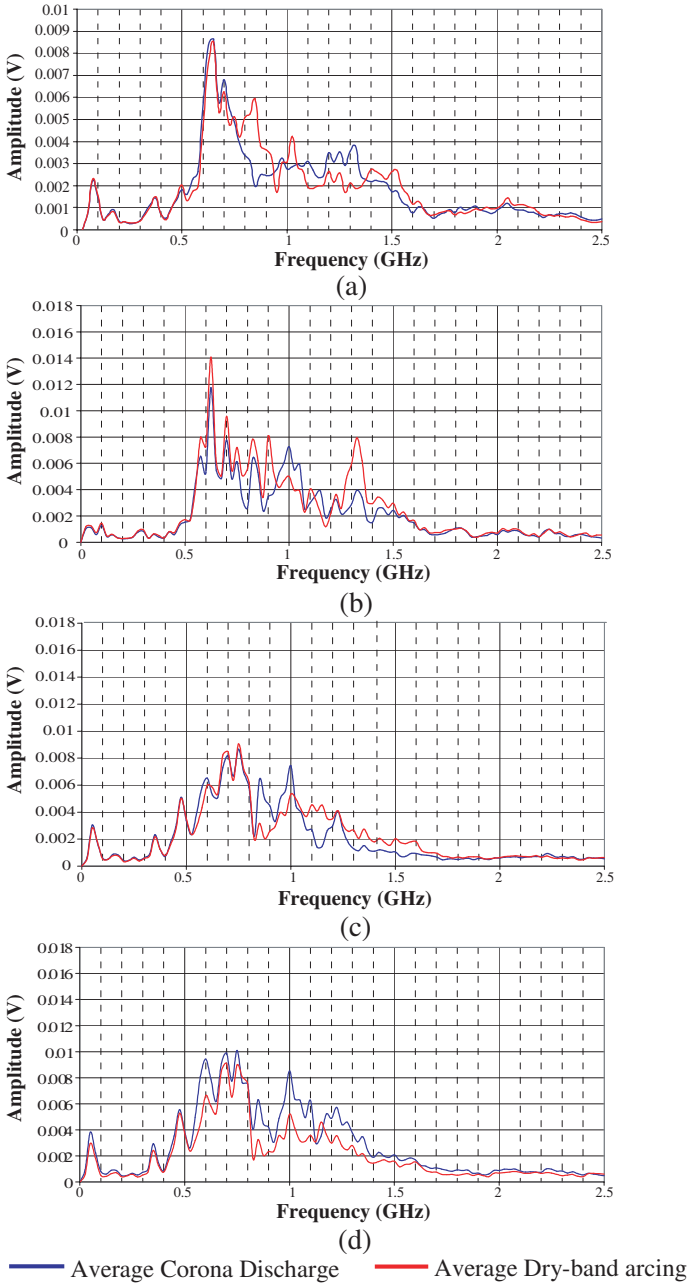

Figure 12. Spectrum of Corona and Dry-band arc discharge at the same position on the insulator surface. (a) 1st Stage. (b) 2nd Stage. (c) 3rd Stage. (d) 4th Stage.

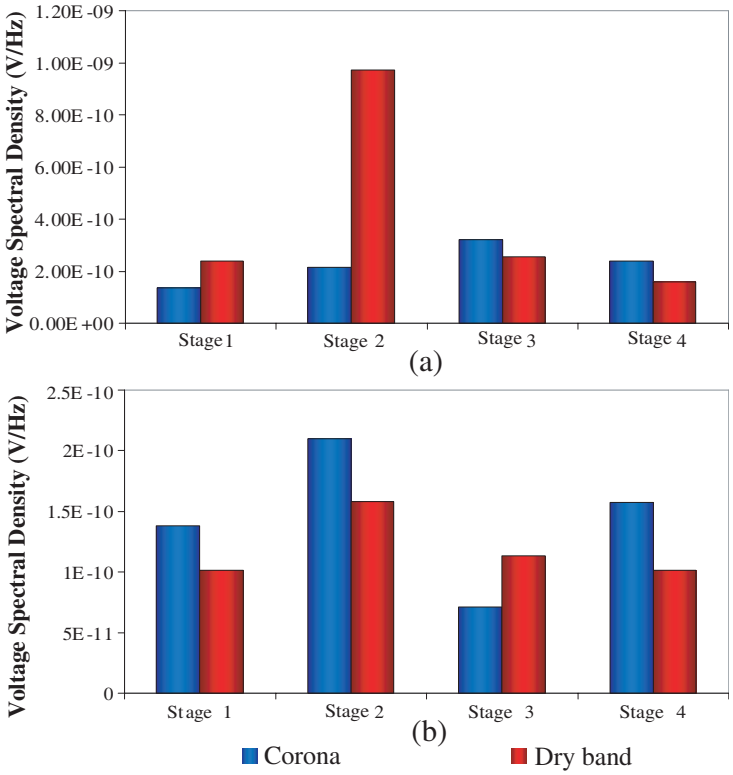

Figure 13. Average Voltage Spectral Density for Corona and Dry-band arc discharges for different contents of water droplets for (a) frequency band of 800 MHz–900 MHz (b) frequency band of 1.25 GHz–1.4 GHz.

Table 2. Approximate contact angle of water droplets for different stages of condition of the insulator.

Stage	Approx. Contact Angle (Degrees)	
	Energized Droplet	Grounded Droplet
1st	71	71
2nd	21	71
3rd	51	47
4th	16	60

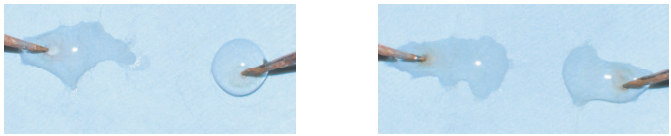

(a) (b)

Figure 14. Shape of the two water droplets (a) 2nd Stage (b) 4th Stage.

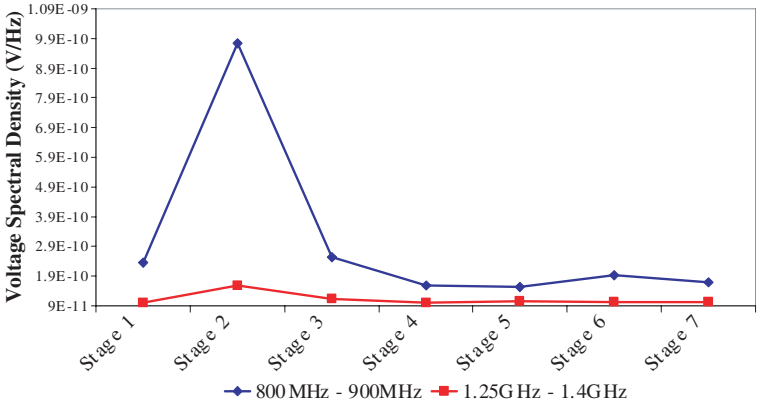

Figure 15. Variation of Voltage Spectral Densities due to dry-band arc discharge in 800 MHz–900 MHz and 1.25 GHz–1.4 GHz bands.

for corona discharge while Stage 3 shows the opposite activity. This unpredictable pattern was caused by the erratic variation of the water droplet footprint and contact angles due to the loss of hydrophobicity, carbonization near electrodes and extensive damage to the insulator surface. Therefore the changes to the shape of water droplets will not be uniform, as shown in the photographs at Stages 2 and 4 in Figure 14. These non-uniform changes to the water droplets are further demonstrated in Table 2, which displays approximate contact angles for the water droplets at each stage up to Stage 4 (after which insulator material completely loses its hydrophobicity).

The voltage spectral density of dry-band arc discharge radiation in the 800 MHz–900 MHz frequency band peaks at Stage 2, then quickly decays, as seen in Figure 15. At Stages 5–7 where the material entirely lost its hydrophobicity, a relatively constant voltage spectral density was detected from the dry-band arc discharges. The 1.25 GHz–1.4 GHz band shows similar behaviour, albeit at a much lower magnitude.

This peak at Stage 2 in 800 MHz–900 MHz band, coupled with the fact that the dry-band arc discharge emissions drop lower than the corresponding corona levels at Stages 3 and 4 (seen in Figure 13(a), could be used to monitor the degradation in surface condition of the insulation material.

4. CONCLUSION

The experimental analysis conducted in this paper has indicated that for uniform water droplets, the transition from corona discharge to dry-band arc discharge can be identified by using RF sensing in the 800 MHz–900 MHz and 1.25 GHz–1.4 GHz bands. The average detected voltage spectral density was shown to be higher for dry-band arc discharges at 800 MHz–900 MHz, whilst corona discharge exhibited stronger levels in the 1.25 GHz–1.4 GHz band. This finding was observed to be independent of water droplet volume and separation for the experiments conducted.

Damage to the insulator surface caused by discharge activity was shown to cause the deformation of water droplets, primarily due to a reduction in hydrophobicity. For an extensively damaged surface it is difficult to observe the transition from corona discharge to dry-band arc discharge as the water droplets immediately wet the surface, eradicating corona. However, it is notionally possible to monitor the degradation of the insulation surface by sensing the reduction of the voltage spectral density due to dry-band arc discharges in the 800 MHz–900 MHz band, and detecting where it drops below the corresponding corona levels. These findings may be employed in a remote monitoring system which detects RF radiation to classify discharges and monitor the condition of HV insulators. Further investigations into the effects of insulator pollution, contaminates and moisture on the discharge radiation need to be explored before such a system could be used in practical scenarios.

ACKNOWLEDGMENT

The authors acknowledge Dr. A. Bojovschi and Dr. A. Galehdar for constructive discussions. The authors would also like to thank EMC Pacific, Australia for providing the epoxy samples which were used in this research. This research was supported under Australian Research Council's Discovery Projects funding scheme (project number DP0880770).

REFERENCES

1. Mackevich, J. and M. Shah, "Polymer outdoor insulating materials. Part I: Comparison of porcelain and polymer electrical insulation," *IEEE Electrical Insulation Magazine*, Vol. 13, 5–12, 1997.
2. Gorur, R., G. Karady, A. Jagota, M. Shah, and A. Yates, "Aging in silicone rubber used for outdoor insulation," *IEEE Transactions on Power Delivery*, Vol. 7, 525–538, 1992.
3. Zhu, Y., M. Otsubo, and C. Honda, "Behavior of water droplet on electrically stressed polymeric coating surface," *Surface and Coatings Technology*, Vol. 201, 5541–5546, Feb. 2007
4. Phillips, A., D. Childs, and H. Schneider, "Aging of nonceramic insulators due to corona from water drops," *IEEE Transactions on Power Delivery*, Vol. 14, 1081–1089, 1999.
5. Gorus, R., E. Cherney, and R. Hackam, "The AC and DC performance of polymeric insulating materials under accelerated aging in a fog chamber," *IEEE Transactions on Power Delivery*, Vol. 3, 1892–1902, 1988.
6. Meyer, L., S. Jayaram, and E. Cherney, "Correlation of damage, dry band arcing energy, and temperature in inclined plane testing of silicone rubber for outdoor insulation," *IEEE Transactions on Dielectrics and Electrical Insulation*, Vol. 11, 424–432, 2004.
7. El-Hag, A. H., "Leakage current characterization for estimating the conditions of non-ceramic insulators' surfaces," *Electric Power Systems Research*, Vol. 77, 379–384, Mar. 2007.
8. Kumagai, S. and N. Yoshimura, "Leakage current characterization for estimating the conditions of ceramic and polymeric insulating surfaces," *IEEE Transactions on Dielectrics and Electrical Insulation*, Vol. 11, 681–690, 2004.
9. Lopes, I., S. Jayaram, and E. Cherney, "A method for detecting the transition from corona from water droplets to dry-band arcing on silicone rubber insulators," *IEEE Transactions on Dielectrics and Electrical Insulation*, Vol. 9, 964–971, 2002.
10. Fernando, S. C., K. L. Wong, and W. S. T. Rowe, "RF radiation from corona discharge between two water droplets on epoxy and silicone-rubber surfaces," *Proceedings of Asia-Pacific Microwave Conference*, 1582–1585, Melbourne, Australia, Dec. 5–8, 2011.
11. Sarathi, R. and G. Nagesh, "UHF technique for identification of discharges initiated by liquid droplet in epoxy nanocomposite insulation material under ac voltages," *Journal of Physics D: Applied Physics*, Vol. 41, 155407, 2008.

12. Higashiyama, Y., S. Yanase, and T. Sugimoto, "DC corona discharge from water droplets on a hydrophobic surface," *Journal of Electrostatics*, Vol. 55, 351–360, Jul. 2002.
13. Imano, A. and A. Beroual, "Study of the behavior of AC discharges of water drops on both conducting and dielectric solid surfaces," *IEEE Transactions on Dielectrics and Electrical Insulation*, Vol. 17, 1569–1575, 2010.
14. Rowland, S. M. and F. C. Lin, "Stability of alternating current discharges between water drops on insulation surfaces," *Journal of Physics D: Applied Physics*, Vol. 39, 3067–3076, 2006.
15. Fernando, S. C., K. L. Wong, A. Bojovschi, and W. S. T. Rowe, "Detection of GHz frequency components of partial discharge in various media," *Proceedings of 16th International Symposium on High Voltage Engineering (ISH 2009)*, 687–692, Cape Town, South Africa, 2009.
16. El-Kishky, H. and R. Gorur, "Electric field computation on an insulating surface with discrete water droplets," *IEEE Transactions on Dielectrics and Electrical Insulation*, Vol. 3, 450–456, 1996.
17. Que, W., "Electric field and voltage distributions along non-ceramic insulators," Ph.D. Dissertation, Ohio State University, 2002.
18. Guan, Z., L. Wang, B. Yang, X. Liang, and Z. Li, "Electric field analysis of water drop corona," *IEEE Transactions on Power Delivery*, Vol. 20, 964–969, 2005.
19. Fujii, O., K. Honsali, Y. Mizuno, and K. Naito, "A basic study on the effect of voltage stress on a water droplet on a silicone rubber surface," *IEEE Transactions on Dielectrics and Electrical Insulation*, Vol. 16, 116–122, 2009.
20. Gao, H., Z. Jia, Y. Mao, Z. Guan, and L. Wang, "Effect of hydrophobicity on electric field distribution and discharges along various wetted hydrophobic surfaces," *IEEE Transactions on Dielectrics and Electrical Insulation*, Vol. 15, 435–443, 2008.
21. Zhu, Y., M. Otsubo, C. Honda, Y. Hashimoto, and A. Ohno, "Mechanism for change in leakage current waveform on a wet silicone rubber surface — A study using a dynamic 3-D model," *IEEE Transactions on Dielectrics and Electrical Insulation*, Vol. 12, 556–565, 2005.
22. Kim, S., E. Cherney, and R. Hackam, "Effect of dry band arcing on the surface of RTV silicone rubber coatings," *IEEE International Symposium on Electrical Insulation*, 237–240, 1992.